

# Geochemical portray of the Pacific Ridge: New isotopic data and statistical techniques

Cédric Hamelin<sup>a,\*</sup>, Laure Dosso<sup>b</sup>, Barry B. Hanan<sup>c</sup>, Manuel Moreira<sup>d</sup>, Andrew P. Kositsky<sup>e</sup> & Marion Y. Thomas<sup>e</sup>

<sup>a</sup> I.U.E.M., U.B.O., Place Nicolas Copernic, 29280 Plouzané, France

<sup>b</sup> Centre National de la Recherche Scientifique, UMR 6538, IFREMER, BP70, 29280 Plouzané, France

<sup>c</sup> Department of Geological Sciences, S.D.S.U., 5500 Campanile Drive, San Diego, CA 92182-1020, USA

<sup>d</sup> Institut de Physique du Globe de Paris, CNRS UMR 7154, 1 rue Jussieu, 75252 Paris CEDEX 05, France

<sup>e</sup> Tectonics Observatory, California Institute of Technology, Pasadena, CA 91125, USA

\* Corresponding author : Cédric Hamelin, I.P.G.P, 1 rue Jussieu, Bureau 345, 75252 Paris CEDEX 05, France. Tel.: +33 1 83 95 76 72; fax: +33 1 7193 7710, email address : hamelin@ipgp.fr

## ABSTRACT:

Samples collected during the PACANTARCTIC 2 cruise fill a sampling gap from 53° to 41° S along the Pacific Antarctic Ridge (PAR). Analysis of Sr, Nd, Pb, Hf, and He isotope compositions of these new samples is shown together with published data from 66°S to 53°S and from the EPR. The recent advance in analytical mass spectrometry techniques generates a spectacular increase in the number of multidimensional isotopic data for oceanic basalts. Working with such multidimensional datasets generates a new approach for the data interpretation, preferably based on statistical analysis techniques.

Principal Component Analysis (PCA) is a powerful mathematical tool to study this type of datasets. The purpose of PCA is to reduce the number of dimensions by keeping only those characteristics that contribute most to its variance. Using this technique, it becomes possible to have a statistical picture of the geochemical variations along the entire Pacific Ridge from 70°S to 10°S. The incomplete sampling of the ridge led previously to the identification of a large-scale division of the south Pacific mantle at the latitude of Easter Island. The PCA method applied here to the completed dataset reveals a different geochemical profile. Along the Pacific Ridge, a large-scale bell-shaped variation with an extremum at about 38°S of latitude is interpreted as a progressive change in the geochemical characteristics of the depleted matrix of the mantle. This Pacific Isotopic Bump (PIB) is also noticeable in the He isotopic ratio along-axis variation. The linear correlation observed between He and heavy radiogenic isotopes, together with the result of the PCA calculation, suggests that the large-scale variation is unrelated to the plume–ridge interactions in the area and should rather be attributed to the partial melting of a marble-cake assemblage.

## Research Highlights

New Sr, Nd, Pb, Hf, and He isotopes data fill a sampling gap along the Pacific Ridge. ► We examine geochemical variation in MORB using a principal component analysis. ► A progressive change in the depleted matrix is recognized along the Pacific ridge. ► In samples devoid of plume influence, He isotopes correlates with Pb isotopes.

**Keywords:** oceanic basalts; Pacific–Antarctic Ridge; mantle heterogeneity; Principal Component Analysis; Sr Nd Pb Hf isotopes

## 44 **1. Introduction**

45 Mid-oceanic ridge basalts (MORB) are the result of continuous melting of the ambient  
46 upper mantle beneath oceanic ridges. The MORB-source mantle is generally thought to have  
47 been depleted ~2 Gy ago by extraction of the continents. Although the range of geochemical  
48 variations in oceanic basalts is mostly attributed to the influence of Ocean Island Basalt  
49 (OIB), significant geochemical heterogeneity in MORB has been recognized (Hoffman et al.,  
50 2003 and reference therein; Rudge et al., 2005). This heterogeneity has been revealed using  
51 radiogenic isotope ratios (Sr, Nd, Pb and Hf) in areas devoid of plume influence. Numerous  
52 studies have attempted to model the mixing relationship between enriched and depleted  
53 domains within the mantle to reproduce the range of isotopic variations observed in oceanic  
54 basalts (Albarède, 2001; Meibom and Anderson, 2004; Rudge et al., 2005; Kellogg et al.,  
55 2007). The range of Sr, Nd and Pb isotopic compositions depends not only on the end-  
56 member compositions but also on the volume of mantle sampled during the melting relative to  
57 the length scale of heterogeneities (Kellogg et al., 2007). Therefore, the range of MORB  
58 geochemical variations reflects the size, the spatial distribution, and the difference of  
59 fusibility of heterogeneities within the upper mantle. In addition to this intrinsic heterogeneity  
60 of the MORB mantle, radiogenic isotope studies have led to the definition of distinct broad  
61 mantle isotopic domains, such as the archetypal DUPAL anomaly located in the south  
62 hemisphere (Dupré and Allègre, 1983; Castillo, 1988). Boundaries between these domains  
63 can be (i) extremely sharp as seen at the Antarctic Australian–Antarctic Discordance (ADD),  
64 with isotopic ratios (Sr, Nd, Pb and Hf) abruptly changing from Indian to Pacific values (Pyle  
65 et al., 1992, Hanan et al., 2004; Meyzen et al., 2007; Cooper et al., 2009) or (ii) more gradual  
66 as seen in the transition from Southwest Indian Ridge to South Atlantic MORB (Meyzen et al.,  
67 2005).

68 Another example of these large geochemical provinces is given by the two sub-pacific  
69 mantle domains (Vlastélic et al., 1999). The distinctive isotopic properties of these large-scale  
70 geochemical domains suggest a long-term isolation of these mantle provinces, each with their  
71 own convective histories involving various amounts of melting residues and recycled  
72 components. On the basis of an incomplete dataset, a boundary between these two Pacific  
73 provinces has been located at the latitude of the Easter Island microplate (Vlastélic et al.,  
74 1999). But in order to have a complete geochemical view of the southern Pacific Ridge from  
75 66 to 10°S, it was necessary to fill the sampling gap between 53°S and 41°S. This became one  
76 of the main objectives of the PACANTARCTIC2 cruise which took place in 2004-05 (Dosso  
77 et al. 2005, Klingelhoefer et al., 2006, Moreira et al., 2008; Hamelin et al., 2010). Analyses of  
78 Sr, Nd, Pb, Hf and He isotopic compositions of these new samples from the Pacific Antarctic  
79 Ridge (PAR) are compiled here together with published data from 66°S to 53°S and from the  
80 East Pacific Rise (EPR). Therefore it becomes possible to have a picture of the geochemical  
81 variations along the entire Pacific Ridge from 66°S to the 10°S. Adapting a Principal  
82 Component Analysis (PCA) to incomplete datasets, we show a detailed portrayal of the  
83 geochemical variability of the Pacific Ridge.

84

## 85 **2. Data selection and analytical methods.**

### 86 *2.1. The Pacific Ridge database from 10 to 66°S.*

87 Along the Pacific Ridge, the Chile Triple Junction at 35°S/110°W separates the PAR from  
88 the EPR. The two Pacific ridges show different geological settings: the full spreading rate  
89 increases along the PAR from 54 mm/yr at 65°S to 100 mm/yr at 35°S whereas it decreases  
90 along the EPR from 158 mm/yr at 35°S to 146 mm/yr at 10°S. In conjunction, the ridge axis  
91 morphology changes from a valley to a dome north of 60°S along the PAR (Ondréas et al.,

92 2001), whereas the EPR is characterized by a uniform dome shaped morphology. Three  
93 plume-ridge interactions generate abnormal morphological structures along this section:  
94 Foundation (~38°S), Easter Island (~26°S) and 17°S. They are recognized by a high ridge  
95 cross-sectional area (Klingelhöfer et al., 2006) and the presence of intense off-axis volcanic  
96 activity. Compared to the EPR, the Pacific Antarctic Ridge still remains geochemically poorly  
97 known. A large portion of this plate boundary has been previously surveyed (Lonsdale, 1994;  
98 Cande et al., 1995) but the northern part has only recently been sampled (Dosso et al., 2005;  
99 Moreira et al., 2008; Hamelin et al., 2010).

100

101 To generate a coherent database along the Pacific ridges, on-axis samples analyzed for one  
102 or more isotopic ratios (Sr-Nd-Pb-Hf-He) are selected from 66°S to 10°S using our new  
103 isotope data (table 1) completed with the petrological database of the Lamont-Doherty Earth  
104 Observatory (<http://www.petdb.org>). In most cases when the reference values of the standards  
105 are reported, the data are normalized to the values of NBS987, 0.71025 for Sr, of JNdi-1,  
106 0.512104 and La Jolla, 0.511852 for Nd, NBS981,  $^{206}\text{Pb}/^{204}\text{Pb}=16.9373$ ,  $^{207}\text{Pb}/^{204}\text{Pb}=15.4925$ ,  
107  $^{208}\text{Pb}/^{204}\text{Pb}=36.7054$ , for Pb and JMC475, 0.282162 for Hf (see [http://georem.mpch-](http://georem.mpch-mainz.gwdg.de/)  
108 [mainz.gwdg.de/](http://georem.mpch-mainz.gwdg.de/) for details and references).:

109

## 110 2.2. Analytical methods.

### 111 2.2.1. Double Spike Pb analyses along the PAR

112 New high-resolution Pb analyses were carried out for samples collected during  
113 PACANTARCTIC1 (PAC1) and PACANTARCTIC2 (PAC2) cruises along PAR segments  
114 from 66°S to 56°S and from 53°S to 41°S respectively (Fig. 1, Table 1). Small chips from the  
115 inner part of the pillow lavas were handpicked to avoid altered surfaces that could be a  
116 potential source of Pb contamination. Powdered samples were leached with 6M HCl at 140°C

117 for an hour and then rinsed up to 6 times with ultrapure water prior to dissolution. Lead  
118 separation was then performed on an anionic exchange resin. Pb analyses were performed at  
119 Ifremer (Centre de Brest) on a Finnigan MAT 26x multicollector instrument (MAT261  
120 upgraded by Spectromat), using the double spike technique with the calibrated Southampton-  
121 Brest 207/204 spike (Ishizuka et al., 2003). Replicate analyses of the Pb isotope standard  
122 NBS981 gave an average of  $16.9432 \pm 0.0027$  and  $15.5004 \pm 0.0029$  and  $36.7326 \pm 0.0086$  for  
123  $^{206}\text{Pb}/^{204}\text{Pb}$ ,  $^{207}\text{Pb}/^{204}\text{Pb}$  and  $^{208}\text{Pb}/^{204}\text{Pb}$ , respectively. Pb blanks measured using this  
124 procedure were  $< 100$  pg, and thus negligible relative to the amount of sample analyzed.

125

### 126 2.2.2. *Hf measurements along the PAR*

127 Hafnium isotopic compositions were analyzed along the PAC1 ridge segments at SDSU on  
128 splits from the same samples (Hamelin et al., 2010). Hf was separated using the protocol of  
129 Blichert-Toft et al. 1997 with a negligible blank of less than 25 pg. Hf isotope ratios were  
130 measured at SDSU using the Nu Plasma. The  $^{176}\text{Hf}/^{177}\text{Hf}$  was normalized for mass  
131 fractionation relative to  $^{179}\text{Hf}/^{177}\text{Hf}=0.7325$ . The JMC-475 Hf standard  $^{176}\text{Hf}/^{177}\text{Hf}$  gave  
132  $0.282160 \pm 0.000010$  ( $2\sigma$ ) during this study. The standard was run alternately with samples to  
133 monitor machine performance.

134

### 135 2.2.3. *He measurements along the PAR*

136 Helium isotopic compositions have been measured on PAC1 and PAC2 samples at IPGP  
137 (Institut de Physique du Globe de Paris). Fresh pieces of glass were cleaned with distilled  
138 water, ethanol and acetone using an ultrasonic bath. Some samples were also cleaned with  
139 hydrogen peroxide in order to remove some Mg crust. Analytical procedure is identical to  
140 previous studies from our laboratory and can be found in Moreira et al. (1995). Samples were  
141 crushed under vacuum with analytical blanks of  $7 \pm 1$  nccSTP  $^4\text{He}$ . This corresponds to 0.02 to

142 0.4% of the samples. Helium concentrations and isotopic composition were measured using  
143 the ARESIBOII mass spectrometer (Moreira et al., 2008).

144

### 145 **3. New results compared to published MORB data along this** 146 **ridge section.**

147

148 These results include samples from 66°S to 56°S (PAC1) and from 53°S to 41°S (PAC2)  
149 (Fig. 1). New high resolution Pb analyses as well as Hf and He analyses are presented here in  
150 Table 1. The Sr, Nd and Hf analyses on the same samples are found in Vlastélic et al. (2000)  
151 and Hamelin et al. (2010).

152

#### 153 *3.1. Binary isotopic correlations*

154 With 7 isotopic ratios, the number of possible binary isotope diagrams is 21. As an  
155 example, we choose here to describe 4 such binary plots, selecting some of the most  
156 commonly discussed (Fig. 2A-D). In all diagrams, pacific MORB samples devoid of plume  
157 influence define linear correlations that in most cases have been previously described in the  
158 literature. This result is in good agreement with the expected coherence in behavior between  
159 Rb-Sr, U-Pb, Th-Pb, Sm-Nd and Lu-Hf isotopic systems compared to each other during  
160 magmatic processes. When plume-ridge interaction samples are included in our dataset, they  
161 define elongated fields overlapping PAR-EPR array except in Figure 2C where He- $\epsilon_{Nd}$   
162 isotopic ratios define sub-parallel trends which emerge from the PAR-EPR array and point  
163 towards higher  $^3\text{He}/^4\text{He}$  (R/Ra) ratios. More than 30 years of He isotopes systematic of  
164 oceanic basalts worldwide have shown that MORB samples are characterized by a narrow

165 range of composition compared to OIB samples. However even within this limited range, our  
166 data show a linear correlation between  $^3\text{He}/^4\text{He}$  (R/Ra) values and  $\epsilon_{\text{Nd}}$  (Fig. 2C). The  
167 correlation between He and other isotopic systems will be discussed further below (§4.4.2).

168 In contrast with the decoupling of Hf and Nd isotope compositions previously documented  
169 in MORB (e.g., Patchett and Tatsumoto, 1980; Salters and White, 1998; Chauvel et al., 2001;  
170 Debaille et al., 2006), a rather good correlation between these two isotopic systems is  
171 observed along our studied area (Fig. 2B). Debaille et al. (2006) have suggested that a  
172 distinctive behavior of Hf during disequilibrium melting along their studied ridge area (Atlantic  
173 ridge 22-35°N) could explain a decoupled behavior of  $^{176}\text{Hf}/^{177}\text{Hf}$  with respect to other  
174 isotopic ratios. The linear correlations observed in our dataset, show that the hypothesis of a  
175 specific behavior of Hf does not apply along the Pacific ridges. Recently, good correlations  
176 between Hf and Nd isotopic ratios have been reported from other ridge segments such as  
177 Mohs Ridge (Blichert-Toft et al., 2005) and the entire mid-Atlantic Ridge (Agranier et al.,  
178 2005).

179

### 180 *3.2. MORB variability along the south Pacific Ridge.*

181 Latitudinal isotopic variations of south Pacific Ridge basalts are shown in Figure 3. An  
182 important geochemical feature from 66 to 10°S is a large scale (spanning approximately  
183 5000km) and coherent variation of all isotopes shown by a bell shape grey line. The  
184 extremum of this variation defining the Pacific Isotopic Bump (PIB), is located at the latitude  
185 of Foundation (38°S). It reveals a less depleted component, characterized by more radiogenic  
186 values for Sr, Pb isotopic ratios, and correlatively less radiogenic values for Nd and Hf. Three  
187 shorter wavelength variations of the order of 200 to 700km are seen as isotopic anomalies  
188 superimposed on the otherwise bell shaped curve of the isotope signature along the ridge. In a  
189 way similar to the Pacific Isotopic Bump, these variations are towards more radiogenic Sr and

190 Pb values and coherently less radiogenic Nd and Hf values. They indicate the influence of  
191 enriched materials due to plume-ridge interactions.

192 Helium isotopes do not fit this Sr-Pb/Hf-Nd coherent behavior. At the latitude of the  
193 Foundation-Ridge intersection (38°S), the bell-shaped He curve shows radiogenic  $^3\text{He}/^4\text{He}$   
194 ratios. But on the other hand, hot-spot influenced samples form negative “plume anomalies”  
195 with very unradiogenic signatures (high  $^3\text{He}/^4\text{He}$  ratios, up to 12 R/Ra). The amplitudes of the  
196 PIB and the anomalies attributed to the plume effect are of the same order of magnitude for  
197 Nd, Hf and Pb. For He and Sr, the PIB has much smaller amplitude than the hotspot  
198 anomalies. Additionally, local MORB variability is expressed as spikes, which are likely  
199 related to transform faults (Eltanin System).

200

## 201 **4. Discussion**

### 202 *4.1 Statistical definition of mantle reference lines*

203 In most binary plots of radiogenic isotopic ratios, representative points of mantle derived  
204 material define linear trends. Historically, these trends have been used to define reference  
205 lines such as the Northern Hemisphere Reference Line (NHRL) in Pb-Pb plot (Hart, 1984) or  
206 the “Mantle Array” in Sr-Nd plot (DePaolo and Wasserburg, 1979) and the Nd-Hf plot  
207 (Vervoort and Blichert-Toft, 1999). These reference lines are arbitrary and depend on the  
208 abundance of data available at the time of their definition. However, the data colinearity in  
209 these plots justifies these convenient choices. The NHRL has been convenient to quantify the  
210 Dupal anomaly using the  $\Delta 7/4$  and  $\Delta 8/4$  (Hart, 1984). In 1999, new MORB data from the  
211 south Pacific lead to the definition of the Pacific Reference Line (PRL) which proved  
212 convenient to compare two sub-pacific mantle domains, using the  $\delta(\text{Nd-Sr})$  and  $\delta(\text{Sr-Pb})$   
213 notations (Vlastélic et al., 1999). With the recent advance in analytical MC-ICPMS

214 techniques, the number of isotopic data increases dramatically. It becomes possible to look at  
215 these reference lines in multidimensional space from a statistical point of view. Principal  
216 Component Analysis (PCA) is a powerful mathematical tool to study data sets such as a  
217 geochemical database including Sr-Nd-Pb-Hf analyses. The purpose of PCA analysis is to  
218 reduce the number of dimensions in a data set by keeping those characteristics that contribute  
219 most to its variance. This technique has been used in previous mantle heterogeneity studies  
220 (e.g. Agranier et al., 2005, Debaille et al., 2006) The PCA method used with our geochemical  
221 dataset has been initially developed for low-rank matrix approximations (Srebro and Jaakkola,  
222 2003) and was recently adapted for tectonic problems using incomplete geodetic times series  
223 (Kositsky and Avouac, 2010). The main difference with traditional PCA methods is that the  
224 singular value decomposition is replaced by a more sophisticated decomposition, which  
225 appropriately takes into account samples with a missing isotope measurement. This technique  
226 is particularly suitable to geochemical data as it allows computing the principal components  
227 using the whole dataset, increasing therefore the accuracy of the calculation (see  
228 supplementary material for a more detailed discussion about the concept and the limits of our  
229 calculation). Although more recently ICA (Independent Component Analysis) has been  
230 chosen by some authors (Iwamori and Albarède, 2008, Iwamori et al., 2010), the preferred  
231 PCA method used here has the advantage of dealing with missing isotopic data, assuming that  
232 decorrelation is still a good assumption of independence in our dataset.

233 Because the PCA method is an orthogonal linear transformation, it assumes the linearity of  
234 the data co-variations. In most binary isotopic diagrams, mixing processes are expressed by  
235 hyperboles whose curvatures depend on the elemental concentration ratios of the involved  
236 end-members. But in the case of MORB, pseudo-linear correlations are observed (Fig. 2)  
237 indicating that denominator elements are in approximately constant proportions in the mixing  
238 components. It is very difficult to evaluate the extent of non-linear relationships concealed

239 within the analytical noise. However, it is worth noting that the geographical variations of the  
240 components calculated with our method are approximately the same as those computed in the  
241 3-dimensional space of Pb isotopes, in which relationships are linear. In order to minimize the  
242 correlations induced by the  $^{204}\text{Pb}$  analytical noise (it represents only about 1.4% of the total  
243 Pb), the computation has been made in the  $^{204}\text{Pb}/^{206}\text{Pb}$ ,  $^{207}\text{Pb}/^{206}\text{Pb}$  and  $^{208}\text{Pb}/^{206}\text{Pb}$  space.  
244 Considering the problematic of our study, this observation suggests that the curvature can be  
245 neglected. One drawback of PCA in general stems from the fact that PCA is a projection  
246 method, and sometimes low-dimensional visualization can lead to erroneous interpretations.

#### 247 *4.2. Distribution of the variance among the principal components.*

248 The most striking result of the PCA is that the first principal component accounts for more  
249 than 70% of the total variance. This result is remarkable considering the number of  
250 geochemical parameters involved in the very large number of samples used in this analysis. It  
251 indicates the strong coherence of all isotopic ratios within the depleted mantle domain. These  
252 correlations in binary plots of isotopic systems are the result of two antagonistic processes  
253 that took place over time: chemical fractionation events leading to the existence of enriched  
254 and depleted mantle reservoirs and mechanical mixing of these reservoirs during mantle  
255 convection. The chemical fractionation between parent and daughter isotopes is controlled by  
256 distribution coefficients. Even if these coefficients can be modified by multiple parameters,  
257 they remain consistent from one element to another. Since these processes are approximately  
258 linear, the resulting dispersion is located along a line corresponding to PC1 (the first Principal  
259 Component).

260 While the importance of the first component is indisputable, one challenge with PCA is to  
261 establish the number of significant components needed to explain the observed data variance.  
262 A classical way to illustrate the number of relevant components is to study the residual  
263 variance ( $\chi^2$ ) obtained for each component (e.g. Kositsky and Avouac, 2010). This value

264 drops abruptly after the third component (see supplementary material). At first, we can infer  
265 that the information brought by the fourth to the sixth principal components is statistically  
266 insignificant and can safely be ignored. Using a PCA computed in the 3-dimensional space of  
267 Pb isotopes, the principal components account for 91.7%, 8.2% and 0.1% of the variance for  
268 PC1, PC2 and PC3 respectively. This observation suggests that the variance expressed by  
269 principal components over the order of 2 is the result of a randomly distributed error. Also the  
270 absence of coherent geographical variation for the third component suggests that this variance  
271 could either be a very local variation or an artifact of our data compilation (i.e. sampling bias,  
272 data and error normalization between different laboratories). This justifies to limit the  
273 discussion of the south pacific mantle heterogeneity to the PC1 and PC2 characteristics.

274

#### 275 *4.3. Mapping geochemical heterogeneities in the mantle using a PCA method.*

276 Using the dataset available at the time, Vlastélic et al. (1999) identified a large  
277 geochemical variation in the south Pacific depleted mantle. Based on an incomplete sampling  
278 of the ridge, they suggested the existence of a sharp boundary located at the latitude of the  
279 Easter Island Microplate (27°S). As an interpretation, they proposed that the Pacific  
280 Superswell divided the mantle into two domains each with their own convective histories,  
281 producing slight differences in their average isotopic signatures. More recently, the origin of  
282 these two domains has been challenged by a model based on plate kinetics (Small and  
283 Danyushevsky, 2003). Small and Danyushevsky proposed that geochemical discontinuities  
284 result from variations of the asthenosphere consumption, which corresponds to the ratio  
285 between the accretion rate and the spreading center migration relative to plumes. Their model  
286 predicted that the fast spreading, slowly migrating East Pacific Rise should have higher  
287 average melting degrees compared to the slower spreading, rapidly migrating Pacific-  
288 Antarctic Rise. In order to identify the two mantle domains along the Pacific Ridge, Vlastélic

289 et al. (1999) used  $\delta(\text{Sr-Pb})$  and  $\delta(\text{Nd-Sr})$ , which are defined as the vertical deviations from  
290 reference lines in Pb vs Sr and Sr vs Nd isotopic ratio plots respectively. These reference  
291 lines (see §4.1) were drawn intuitively in the greatest variance of their dataset. They can be  
292 directly compared to our first principal component. By construction, whatever the number of  
293 dimensions considered in the PCA, the projection of PC1 in a binary diagram resembles the  
294 relevant reference line (Fig. 2). Because PC2 is orthogonal to the greatest variance, sample  
295 values along this component are correlated to delta notations such as  $\delta(\text{Sr-Pb})$ ,  $\delta(\text{Nd-Sr})$  or  
296  $\Delta 8/4\text{Pb}$ . But compared to delta notations, PC2 has the advantage of being rigorously and  
297 statistically determined in a multidimensional isotopic space. The application of the PCA  
298 method to our data compilation (excluding He isotopes) reveals a geochemical profile of the  
299 Pacific Ridge. The plot of PC1 versus latitude summarizes all the characteristics noted with  
300 the different isotopic systems (Fig. 4). The short scale geochemical variations associated with  
301 hotspots as well as the large-scale variation are clearly visible. 17°S and 25°S (Easter Island)  
302 are well defined by sharp anomalies superimposed on the bell shaped curve. A plot of PC2  
303 versus latitude shows a very different picture (Fig. 4): only the large scale variation is  
304 expressed by this component, the geochemical variations associated with hotspots are  
305 flattened and the corresponding samples are projected along the bell shape curve defining the  
306 Pacific Isotopic Bump. This PIB is also shown on plots of delta versus latitude, illustrating the  
307 equivalence of these parameters and PC2 (Fig. 4). At the Juan Fernandez/Foundation latitude  
308 (36°S), the isotopic variation curve reaches an extreme which corresponds to a less “depleted”  
309 isotopic signature. In contrast with the conclusion of Vlastélic et al. (1999), we proposed that  
310 geochemical variations along the Pacific Ridge are not the result of two separated mantle  
311 domains but should rather be seen as a progressive variation of the isotopic composition of the  
312 sub-Pacific depleted mantle. Since the asthenosphere consumption varies abruptly at the Chile  
313 triple junction and is almost constant along the PAR, the plate kinematic model of Small and

314 Danyushevsky (2003) is also inconsistent with the observed progressive variation of the  
315 MORB depleted matrix.

316

317 *4.4. Mixing relationship within the depleted mantle compared to ridge-hotspot*  
318 *interactions.*

319 *4.4.1. Asthenospheric versus hotspots signals as illustrated by Sr-Nd-Pb-Hf.*

320 Except in figures involving He isotopes, geochemical variations related to ridge/hotspot  
321 interactions are consistent with variations of samples devoid of plume influence. At first, it is  
322 difficult to distinguish the two types of variations in binary isotopic plots (Fig. 2).  
323 Nevertheless, a PCA computed with all heavy radiogenic isotopes clearly illustrate a  
324 difference: hotspot signatures are exclusively visible with PC1, while the variance related to  
325 the large scale variation (PIB) is illustrated by both PC1 and PC2 versus latitude (Fig. 4). In  
326 PC1 versus PC2 space, the MORB field extends from the depleted end member of the mantle  
327 (DMM) toward a recycled oceanic crust end member with a HIMU affinity (Fig. 5). The  
328 samples identified as resulting from a plume-ridge interaction are not part of this “depleted  
329 trend”. Rather their data field extends from the depleted trend towards more enriched-type  
330 end members such as C and/or EM. This observation supports the idea that the large scale  
331 variation in the depleted Pacific mantle is unrelated to ridge/hotspot interactions. This  
332 variation is therefore equivalent to the intrinsic variability of MORB recognized in other areas  
333 (e.g. Dosso et al., 1999, Donnelly et al., 2004; Debaille et al., 2006; Hémond et al., 2006). It  
334 has to be noted that PCA calculations assume a linearity criteria which is not satisfied when  
335 dealing with isotopic compositions of the mantle end-members. It is thus not possible to  
336 determine more precisely the nature of the different mantle components responsible for the  
337 observed trends. Nevertheless, the PCA calculations establish that the progressive

338 geochemical change of the depleted matrix of the Pacific mantle is not the result of hotspot  
339 material being diluted into the depleted mantle. Using a different approach, Meyzen et al.  
340 (2007) successfully unscrambled the hotspot and asthenospheric signals. These authors have  
341 proposed that the geochemical variations unrelated to ridge/hotspot interactions along the  
342 South West Indian ridge and the South Atlantic ridge are related to a broad lower mantle  
343 upwelling in this area. Similarly, a broad lower mantle input could be a plausible cause of the  
344 Pacific Isotopic Bump associated with the high spreading rates in the vicinity of the Chile  
345 Ridge Triple junction.

346 It is interesting to compare the results of our PCA calculation along the Pacific ridge with  
347 the spectral analysis performed along the Atlantic ridge by Agranier et al. (2005). These  
348 authors found two contrasting types of spectra along their study area. The first type is  
349 associated with ridge-hotspot interactions and is seen in the first principal component. The  
350 second type is illustrated by the continuous power decrease with the decreasing wavelength of  
351 the second principal component. Agranier et al. (2005) have interpreted this second type of  
352 spectra, unrelated to hotspots, as being the result of the continuous size reduction of mantle  
353 heterogeneities upon stretching and refolding of the convecting mantle. Despite the  
354 differences in geological settings between the Pacific ridge and the Atlantic ridge, our  
355 observations are in good agreement with the statistical analysis of Agranier et al. (2005). We  
356 view the PIB as the consequence of a progressive change in the relative proportions of the  
357 marble-cake components present in the Pacific upper mantle. In this model, hotspot anomalies  
358 are superimposed on the intrinsic mantle heterogeneity expressed in MORB.

359

#### 360 *4.4.2. He isotopes in the depleted mantle compared to hotspot signals.*

361 Unlike other isotopic systems, helium shows a first order discrepancy between the hotspot  
362 and the depleted mantle signals in our studied area (Fig. 3 and Fig. 6): the large scale variation

363 associated to the depleted mantle is characterized by an increase towards more radiogenic  
364 (low  $^3\text{He}/^4\text{He}$ ) compositions, whereas the short scale variation associated to the mantle plumes  
365 points towards high  $^3\text{He}/^4\text{He}$  values as previously noted in Hanan and Graham (1996). The  
366 origin of the large range of elevated  $^3\text{He}/^4\text{He}$  values in OIB lavas is a long-lived controversial  
367 question (Kurz et al., 1982; Allègre et al., 1983; Meibom et al., 2003; Moreira et al., 2004).  
368 Historically, the requirement of a high  $^3\text{He}/^4\text{He}$  reservoir for the OIB lead to the idea that  
369 plumes are tapping a deep, undegassed lower mantle, isolated from the upper mantle  
370 convection (O'Nions et al., 1996; Allègre et al., 1997). Numerous alternative models have  
371 tried to solve the apparent inconsistency between the high  $^3\text{He}/^4\text{He}$  ratio in plumes and the  
372 requirement of a source previously processed through partial melting (e.g. Parman et al.,  
373 2005; Class and Goldstein, 2005; Purtika, 2008; Albarède, 2008; Davies, 2010).

374 Compared to plume-influenced samples, systematics of He isotopes in depleted MORB  
375 samples have shown a very restricted range of  $^3\text{He}/^4\text{He}$  with a peak of distribution around  $8\pm 1$   
376 (R/Ra) (Allègre et al., 1995). Within the uncontaminated depleted mantle sampled along our  
377 studied area,  $^3\text{He}/^4\text{He}$  varies from 6 to 9.5 (R/Ra). Samples devoid of plume influence fall  
378 along a negative trend toward low  $^3\text{He}/^4\text{He}$  values and high  $^{206}\text{Pb}/^{204}\text{Pb}$ . This variation of He  
379 isotopes in our samples devoid of plume influence is clearly related to the PIB identified  
380 along the pacific ridge using PCA with Sr, Nd, Pb and Hf isotopes. It is interesting to note  
381 that the most enriched samples from this correlation show the lowest  $^3\text{He}/^4\text{He}$  values (more  
382 radiogenic). In order to reconcile the  $^3\text{He}/^4\text{He}$  variations with variations of Sr, Pb, Nd and Hf  
383 isotopes, new models take into account the physical specificities of He compared to heavy  
384 radiogenic isotopes: its diffusivity in mantle conditions and its capacity to be outgassed from  
385 melts at sub-surface pressure (e.g. Hart et al., 2008; Albarède et al., 2008; Gonnermann and  
386 Mukhopadhyay, 2009). We propose that the melting of a marble-cake upper mantle,  
387 unpolluted by plumes, produces the good correlation observed between He and Pb isotopes in

388 our depleted samples. The less depleted component of the mantle assemblage is characterized  
389 by a high Pb isotopic ratio and a low  $^3\text{He}/^4\text{He}$  ratio. We suggest that this component was  
390 derived from the recycling of an extensively outgassed oceanic crust. When the oceanic crust  
391 is subducted back into the mantle, it contains negligible concentration of mantle-derived He  
392 (Staudacher and Allègre, 1988). With time, this very low  $^3\text{He}/(\text{U}+\text{Th})$  in subducted slabs is  
393 expected to produce the end-member with high Pb isotopes value and low  $^3\text{He}/^4\text{He}$  ratio (Fig.  
394 6).

395 In our model, the variation of He isotopes along the Pacific ridge could be interpreted as:  
396 (1) a smaller contribution of the refractory layers (less radiogenic), corresponding to a lower  
397  $^3\text{He}/^4\text{He}$  ratio at the PIB but because the melting rate is expected to be higher near the Chile  
398 Ridge Triple Junction, this hypothesis seems very unlikely, or (2) a higher volume of the  
399 recycled end-member in this area. This hypothesis is in agreement with the conclusions  
400 derived from the PCA based on heavy radiogenic isotopes (§4.4.1). The intrinsic geochemical  
401 variation of the depleted upper mantle comforts the image of a marble cake mantle composed  
402 of a refractory component and a recycled oceanic crust component. A broad volume of  
403 recycled component associated with the high spreading rates in the vicinity of the Chile Ridge  
404 Triple junction is therefore a plausible cause of the Pacific Isotopic Bump. The correlation  
405 between He and Pb isotopes revealed by our new data (Fig. 6) suggests that the depleted  
406 mantle is the outcome of a mixing of a different nature than the one involved in the plume-  
407 ridge interaction.

408

409

## 410 **5. Conclusion**

411 Analyses of this new sampling of the PAR complete the dataset of the Pacific Ridge.  
412 Therefore it becomes possible to have a picture of the geochemical variations from 10 to  
413 70°S. Our data show a clear geographical evolution of isotopic characteristics along the  
414 Pacific Ridge. In binary isotopic plots, this large-scale variation is expressed by correlations  
415 between each isotopic dimension. This observation holds true even for the Nd-Hf system  
416 previously reported as decoupled for MORB samples (Debaille et al., 2006). Even more  
417 significant in this study is the linear correlation shown in the isotopic He-Nd and  $^3\text{He}/^4\text{He}$  -  
418  $^{206}\text{Pb}/^{204}\text{Pb}$  plots. In these isotopic spaces, the samples affected by plume-ridge interactions  
419 depart clearly from the linear correlations displayed by the ridge samples coming from the  
420 depleted mantle.

421 Despite the paucity of combined Sr-Nd-Pb-Hf isotope data on individual samples, the PCA  
422 algorithms used here allow us to portray the variation along a huge section of the Pacific  
423 Ridge from a statistical point of view. Compared to previous studies of the sub-Pacific  
424 mantle, the application of PCA reveals a Pacific Isotopic Bump, which can be seen as a  
425 progressive geochemical variation of the depleted upper-mantle matrix rather than a sharp  
426 frontier between two mantle domains. Combining PCA results with the information given by  
427 He isotopes, we suggest that the Pacific Isotopic Bump is unrelated to plume-ridge  
428 interactions. This geochemical variation in the upper mantle reservoir is the result of a  
429 marble-cake mantle assemblage composed of a residual mantle component and a recycled  
430 oceanic crust component.

431

432 **Acknowledgements**

433 The Pb isotope work was funded by CNRS/INSU. The Hf isotope work was supported by  
434 NSF grants to B.B. Hanan. We thank Joan Miller for technical assistance at SDSU. We  
435 acknowledge Rick Carlson for the editorial handling, Francis Albarède and an anonymous  
436 reviewer for constructive comments. Cedric Hamelin thanks the Caltech Tectonic  
437 Observatory for its hospitality during his stay in Pasadena. We gratefully acknowledge Neus  
438 Sabater for her valuable comments.

439

440 **References**

- 441 Agranier, A., Blichert-Toft, J., Graham, D., Debaille, V., Schiano, P., Albarede, F., 2005. The  
442 spectra of isotopic heterogeneities along the mid-Atlantic Ridge. *Earth Planet. Science*  
443 *Lett.*, 238(1-2): 96-109.
- 444 Albarède, F., 2001. Radiogenic ingrowth in systems with multiple reservoirs: applications to  
445 the differentiation of the mantle-crust system. *Earth Planet. Science Lett.*, 189(1-2):  
446 59-73.
- 447 Albarède, F., 2008. Rogue mantle Helium and Neon. *Science*, 319: 943-945.
- 448 Allègre, C.J., Staudacher, T., Sarda, P., Kurz, M., 1983. Constraints on evolution of the earth's  
449 mantle from rare gas systematic. *Nature*, 303: 762-766.
- 450 Allegre, C.J., Moreira, M., Staudacher, T., 1995.  $4\text{He}/3\text{He}$  dispersion and mantle convection.  
451 *Geophysical Research Letters*, 22(17): 2325-2328.
- 452 Allègre, C.J., 1997. Limitation on the mass exchange between the upper and lower mantle: the  
453 evolving convection regime of the Earth. *Earth Planet. Science Lett.*, 150(1-2): 1-6.
- 454 Blichert-Toft, J., Albarède, F., 1999. Hf isotopic compositions of the Hawaii Scientific  
455 Drilling Project core and the source mineralogy of Hawaiian basalts. *Geophys. Res.*  
456 *Lett.*, 26(7): 935-938.
- 457 Blichert-Toft, J., Agranier, A., Andres, M., Kingsley, R., Schilling, J.-G., Albarède, F., 2005.  
458 Geochemical segmentation of the Mid-Atlantic Ridge north of Iceland and ridge-hot  
459 spot interaction in the North Atlantic. *Geochem. Geophys. Geosyst.*, 6(1): Q01E19.
- 460 Cande, S.C., Raymond, C.A., Stock, J. and Haxby, W.F., 1995. Geophysics of the Pitman  
461 fracture zone and Pacific-Antarctic plate motions during the Cenozoic. *Science*, 270:  
462 947-953.
- 463 Chauvel, C., Blichert-Toft, J., 2001. A hafnium isotope and trace element perspective on  
464 melting of the depleted mantle. *Earth Planet. Science Lett.*, 190(3-4): 137-151.
- 465 Class, C., Goldstein, S., 2005. Evolution of helium isotopes in the Earth's mantle. *Nature*,  
466 436(25): 1107-1112.
- 467 Class, C., 2008. Hot arguments to cool off the plume debate? *Geology*, 36(4): 335-336.
- 468 Cooper, K.M., Eiler, J.M., Sims, K.W.W., Langmuir, C.H., 2009. Distribution of recycled  
469 crust within the upper mantle: Insights from the oxygen isotope composition of  
470 MORB from the Australian-Antarctic Discordance. *Geochem. Geophys. Geosyst.*, 10.

471 Davis, 2010. Noble gases in the dynamic mantle. *Geochem. Geophys. Geosyst.*, 11(3):  
472 Q03005.

473 Debaille, V., Blichert-Toft, J., Agraniér, A., Doucelance, R., Schiano, P., Albarède, F., 2006.  
474 Geochemical component relationships in MORB from the Mid-Atlantic Ridge, 22-  
475 35°N. *Earth Planet. Science Lett.*, 241(3-4): 844-862.

476 DePaolo, D.J., Wasserburg, G.J., 1979. Sm-Nd age of the Stillwater complex and the mantle  
477 evolution curve for neodymium. *Geochim. Cosmochim. Acta*, 43: 999-1008.

478 Dosso, L., Bougault, H., Langmuir, C., Bollinger, C., Bonnier, O., Etoubleau, J., (1999). The  
479 age and distribution of mantle heterogeneity along the Mid-Atlantic Ridge (31-41°N).  
480 *Earth Planet. Science Lett.*, 170: 269-286.

481 Dosso, L., Ondréas, H., Briaies, A., Fernagu, P., Floch, G., Hamelin, C., Hanan, B.B.,  
482 Klingelhoefer, F., Moreira, M., Normand, A., 2005. The Pacific-Antarctic Ridge  
483 between 41°15'S and 52°45'S: Survey and sampling during the PACANTARCTIC 2  
484 cruise. *InterRidge News*, 14: 1-5.

485 Dupré, B., Allègre, C.J., 1983. Pb-Sr isotope variation in Indian Ocean basalts and mixing  
486 phenomena. *Nature*, 303: 142-146.

487 Farley, K.A., Neroda, E., 1998. Noble gases in the Earth's mantle. *Annual Review of Earth  
488 and Planetary Sciences*, 26: 189-218.

489 Gonnermann, H.M., Mukhopadhyay, S., 2009. Preserving noble gases in a convecting mantle.  
490 *Nature*, 459: 560-563.

491 Hamelin, C., Dosso, L., Hanan, B., Barrat, J.-A., Ondréas, H., 2010. Sr-Nd-Hf isotopes along  
492 the Pacific Antarctic Ridge from 41 to 53°S. *Geophys. Res. Lett.*, 37(10): L10303.

493 Hanan, B.B., Graham, D.W., 1996. Lead and Helium Isotope Evidence from Oceanic Basalts  
494 for a Common Deep Source of Mantle Plumes. *Science*, 272: 991-995.

495 Hanan, B.B., Blichert Toft, J., Pyle, D.G., Christie, D.M., 2004. Contrasting origins of the  
496 upper mantle revealed by hafnium and lead isotopes from the Southeast Indian Ridge.  
497 *Nature*, 432: 91-94.

498 Hart, S.R., 1984. A large scale isotope anomaly in the Southern Hemisphere mantle. *Nature*,  
499 309: 753-757.

500 Hart, S.R., Kurz, M.D., Wang, Z., 2008. Scale length of mantle heterogeneities: Constraints  
501 from helium diffusion. *Earth Planet. Science Lett.*, 269(3-4): 508-517.

502 Hémond, C., Hofmann, A.W., Vlastélic, I., Nauret, F., 2006. Origin of MORB enrichment and  
503 relative trace element compatibilities along the Mid-Atlantic Ridge between 10° and  
504 24°N. *Geochem. Geophys. Geosyst.*, 7, Q12010.

505 Hofmann, A.W., 2003. Sampling mantle heterogeneity through oceanic basalts: Isotopes and  
506 trace elements. In: H. Holland and K.K. Turekian (Editors), *Treatise on Geochemistry*.  
507 Elsevier-Pergamon, Oxford, pp. 61-101.

508 Iwamori, H., Albarède, F., 2008. "Decoupled isotopic record of ridge and subduction zone  
509 processes in oceanic basalts by independent component analysis." *Geochem. Geophys.*  
510 *Geosyst.*, 9.

511 Iwamori, H., Albarède, F., Nakamura, H., 2010. "Global structure of mantle isotopic  
512 heterogeneity and its implications for mantle differentiation and convection." *Earth*  
513 *Planet. Science Lett.*, 299(3-4): 339-351.

514 Ishizuka, O., Taylor, R.N., Milton, J.A., Nesbitt, R.W., 2003. Fluid-mantle interaction in an  
515 intra-oceanic arc: constraints from high-precision Pb isotopes. *Earth Planet. Science*  
516 *Lett.*, 211: 221-236.

517 Jackson, M.G., Hart, S.R., Saal, A.E., Shimizu, N., Kurz, M.D., Blusztajn, J.S., Skovgaard,  
518 A.C., 2008. Globally elevated titanium, tantalum, and niobium (TITAN) in ocean  
519 island basalts with high  $^3\text{He}/^4\text{He}$ . *Geochem. Geophys. Geosyst.*, 9(4): 1-21.

520 Jackson, M.G., Kurz, M.D., Hart, S.R., 2009. Helium and neon isotopes in phenocrysts from  
521 Samoan lavas: Evidence for heterogeneity in the terrestrial high  $\text{He-3}/\text{He-4}$  mantle.  
522 *Earth Planet. Science Lett.*, 287(3-4): 519-528.

523 Kellogg, J.B., Jacobsen, S.B., O'Connell, R.J., 2007. Modeling lead isotopic heterogeneity in  
524 mid-ocean ridge basalts. *Earth Planet. Science Lett.*, 262(3-4): 328-342.

525 Klein, E.M., Langmuir, C.H., Zindler, A., Staudigel, H., Hamelin, B., 1988. Isotope evidence  
526 of a mantle convection boundary at the Australian-Antartic discordance. *Nature*, 333:  
527 623-629.

528 Klingelhoefer, F., Ondréas, H., Briais, A., Hamelin, C., Dosso, L., 2006. New structural and  
529 geochemical observations from the Pacific-Antarctic Ridge  $52^\circ 45'\text{S}$  and  $41^\circ 15'\text{S}$ .  
530 *Geophys. Res. Lett.*, 33.

531 Kositsky, A.P., Avouac, J.P., 2010. Inverting geodetic time series with a principal component  
532 analysis-based inversion method. *J. Geophys. Res.*, 115(B3): B03401.

533 Kurz, M.D., Jenkins, W.J., Hart, S.R., 1982. Helium isotopic systematics of oceanic islands  
534 and mantle heterogeneity. *Nature*, 297: 43-47.

535 Lonsdale, P., 1994. Geomorphology and structural segmentation of the crest of the southern  
536 (Pacific-Antarctic) East Pacific Rise. *J. Geophys. Res.*, 99(B3): 4683-4702.

537 Meibom, A., Anderson, D.L., Sleep, N.H., Frei, R., Chamberlain, C.P., Hren, M.T., Wooden,  
538 J.L., 2003. Are high  $^3\text{He}/^4\text{He}$  ratios in oceanic basalts an indicator of deep-mantle  
539 plume components? *Earth Planet. Science Lett.*, 208(3-4): 197-204.

540 Meibom, A., Anderson, D.L., 2004. The statistical upper mantle assemblage. *Earth Planet.*  
541 *Science Lett.*, 217(1-2): 123-139.

542 Meyzen, C.M., Ludden, J.N., Humler, E., Luais, B., Toplis, M.J., Mével, C., Storey, M.,  
543 2005. New insights into the origin and distribution of the DUPAL isotope anomaly in  
544 the Indian Ocean mantle from MORB of the Southwest Indian Ridge. *Geochem.*  
545 *Geophys. Geosyst.*, 6(11): 1-34.

546 Meyzen, C.M., Blichert-Toft, J., Ludden, J.N., Humler, E., Mevel, C., Albarede, F., 2007.  
547 Isotopic portrayal of the Earth's upper mantle flow field. *Nature*, 447(7148): 1069-  
548 1074.

549 Moreira, M., Staudacher, T., Sarda, P., Schilling, J.-G., Allègre, C.J., 1995. A primitive plume  
550 neon component in MORB: The Shona ridge-anomaly, South Atlantic (51-52°S),  
551 *Earth Planet. Science Lett.*, 133, 367-377.

552 Moreira, M., Dosso, L., Ondréas, H., 2008. Helium isotopes on the Pacific-Antarctic ridge  
553 (52.5-41.5°S). *Geophys. Res. Lett.*, 35(L10306): 1-6.

554 Ondréas, H., Aslanian, D., Géli, L., Olivet, J.-L. and Briais, A., 2001. Variations in axial  
555 morphology, segmentation, and seafloor roughness along the Pacific-Antarctic Ridge  
556 between 56°S and 66°S. *J. Geophys. Res.*, 106(B5): 8521-8546.

557 O'Nions, R.K., Peltier, W.R., Davies, J.H., Runcorn, S.K., 1996. Phase-transition modulated  
558 mixing in the mantle of the Earth - Discussion. *Philosophical Transactions of the*  
559 *Royal Society of London Series A - Mathematical Physical and Engineering Sciences*,  
560 354(1711): 1443-1447.

561 Parman, S.W., Kurz, M.D., Hart, S.R., Grove, T.L., 2005. Helium solubility in olivine and  
562 implications for high  $^3\text{He}/^4\text{He}$  in ocean island basalts. *Nature*, 437(7062): 1140-1143.

563 Patchett, P.J., Tatsumoto, M., 1980. Hafnium isotope variations in oceanic basalts. *Geophys.*  
564 *Res. Lett.*, 7: 1077-1080.

565 Putirka, K., 2008. Excess temperatures at ocean islands: Implications for mantle layering and  
566 convection. *Geology*, 36(4): 283-286.

567 Pyle, D.G., Christie, D.M., Mahoney, J.J., 1992. Resolving an isotopic boundary within the  
568 Australian-Antarctic Discordance. *Earth Planet. Science Lett.*, 112: 161-178.

569 Rudge, J.F., McKenzie, D., Haynes, P.H., 2005. A theoretical approach to understanding the  
570 isotopic heterogeneity of mid-ocean ridge basalt. *Geochim. Cosmochim. Acta*, 69(15):  
571 3873-3887.

572 Salters, V.J.M., White, W.M., 1998. Hf isotope constraints on mantle evolution. *Chem. Geol.*,  
573 145: 447-460.

574 Small, C., Danyushevsky, L.V., 2003. Plate-kinematic explanation for mid-oceanic-ridge  
575 depth discontinuities. *Geology*, 31(5): 399-402.

576 Srebro, N. N., Jaakkola T. 2003, Weighted low-rank approximations, paper presented at 20th  
577 International Conference on Machine Learning, Assoc. for the Adv. of Art. Intell.,  
578 Washington, D. C.

579 Stracke, A., Bourdon, B., 2009. The importance of melt extraction for tracing mantle  
580 heterogeneity. *Geochim. Cosmochim. Acta*, 73(1): 218-238.

581 Starkey, N.A., Stuart, F.M., Ellam, R.M., Fitton, J.G., Basu, S., Larsen, L.M., 2009. Helium  
582 isotopes in early Iceland plume picrites: Constraints on the composition of high He-  
583 <sup>3</sup>/He-<sup>4</sup> mantle. *Earth Planet. Science Lett.*, 277(1-2): 91-100.

584 Staudacher, T., Allègre, C.J., 1988. Recycling of oceanic crust and sediments: the noble gas  
585 subduction barrier. *Earth Planet. Science Lett.*, 89(2): 173-183.

586 Vlastélic, I., Aslanian, D., Dosso, L., Bougault, H., Olivet, J.L., Géli, L., 1999. Large-scale  
587 chemical and thermal division of the Pacific mantle. *Nature*, 399(6734): 345-350.

588 Vlastélic, I., Dosso, L., Bougault, H., Aslanian, D., Géli, L., Etoubleau, J., Bohn, M., Joron,  
589 J.L., Bollinger, C., 2000. Chemical systematics of an intermediate spreading ridge:  
590 The Pacific-Antarctic Ridge between 56°S and 66°S. *J. Geophys. Res.*, 105(B2):  
591 2915-2936.

592 Vervoort, J.D, Blichert-Toft, J, 1999. Evolution of the depleted mantle: Hf isotope evidence  
593 from juvenile rocks through time, *Geochim. Cosmochim. Acta*, 63, 553-556.

594

595 **Figure captions**

596

597 **Figure 1:** Map of the south pacific basin showing the location of the PACANTARCTIC1 and  
598 PACANTARCTIC2 cruises with respect to the Pacific Antarctic Ridge (PAR) and the East  
599 Pacific Rise (EPR). Hotspot locations are shown in orange on the map.

600

601 **Figure 2:** Examples of binary plots showing correlations within the MORB field. Samples  
602 devoid of plume influence are shown in blue whereas samples from plume-ridge interactions  
603 are in red. Blue circles represent samples collected along the PAR and blue crosses for EPR  
604 samples (all symbols are kept the same in all figures). Mantle reference lines defined in the  
605 literature are shown in dashed lines: in the Sr/Nd plot (A), the Pacific Reference Line (PRL)  
606 (Vlastélic et al., 1999), in the Nd/Hf plot (B), the mantle array (Vervoort et al., 1999), in the  
607 Pb/Pb plot (D), the North Hemisphere Reference Line (NHRL) (Hart, 1984). Since no  
608 reference line had yet been recognized in plots involving He isotopes, we show here a  
609 regression line ( $^3\text{He}/^4\text{He} = 0.63 \varepsilon_{\text{Nd}} + 1.74$ ,  $r = 0.89$ ) (C). The projection of the two first  
610 principal components (PC1 and PC2) calculated in our study are shown (solid black and grey  
611 lines, see text for additional information). Data references can be found in supplementary  
612 materials.

613

614 **Figure 3:** Geochemical variations along the PAR and the EPR from 66°S to 10°S. Dashed  
615 lines represent the location of major transform faults in the area and a grey shade is used for  
616 the Juan Fernandez and Easter Island microplates. The grey curve underlines the large-scale  
617 isotopic variation along the pacific ridges from 10 to 66°S and defines the Pacific Isotopic  
618 Bump (PIB).

619

620 **Figure 4:** Plot of the two first principal components along the Pacific Ridge. The similarity  
621 between PC2 and  $\delta$  notation is illustrated by plotting  $\delta(\text{Sr-Pb})$  as defined by Vlastélic et al.  
622 (1999) and  $\Delta^{207}\text{Pb}$  as defined by Hart (1984) versus latitude.

623

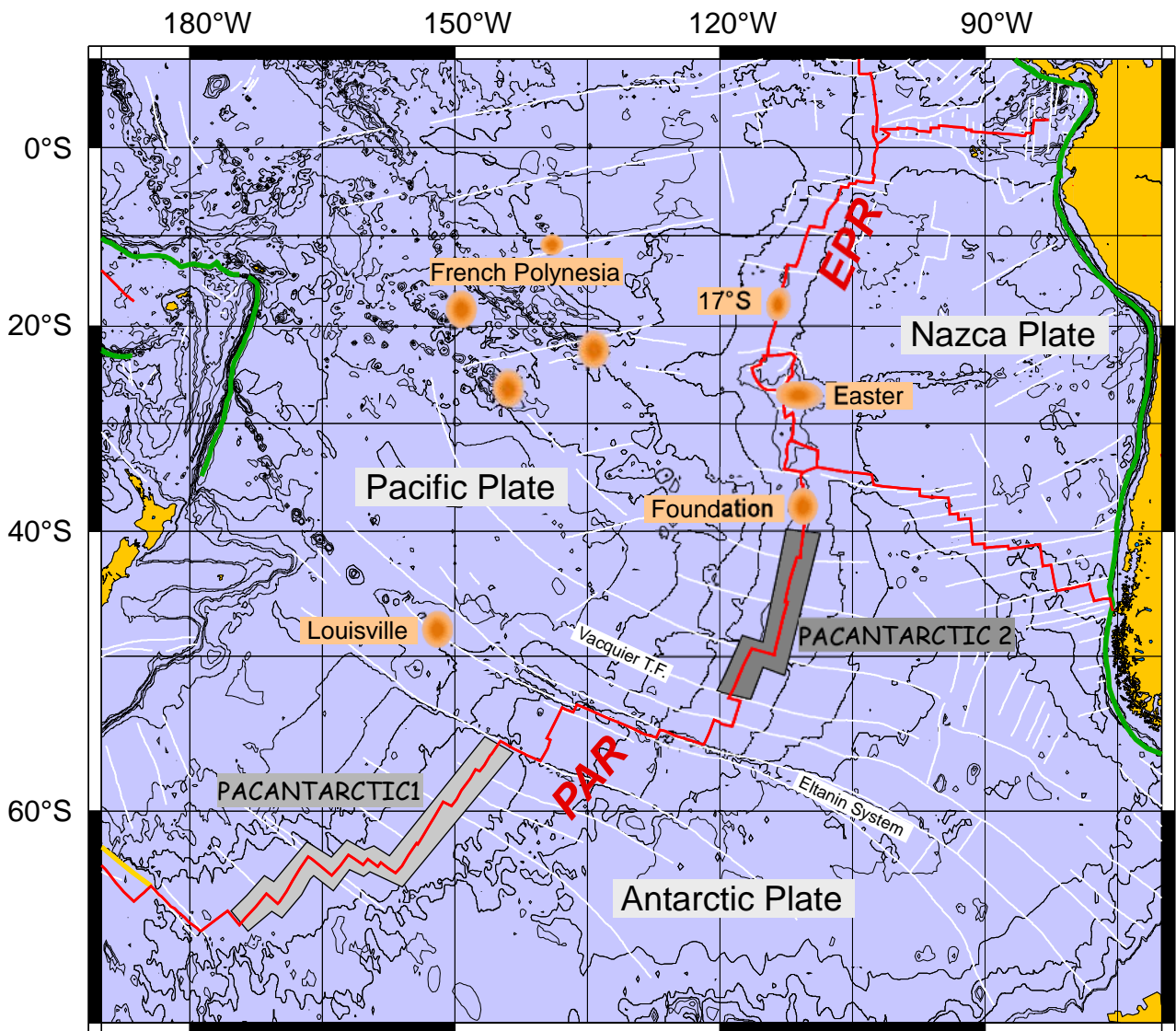
624 **Figure 5:** Plot of PC2 versus PC1 for a principal component analysis computed using Sr, Nd,  
625 Hf and Pb isotopes. The hashed blue field defines the depleted trend and includes EPR and  
626 PAR samples. Data points are drawn as ellipses representing the 95% confidence domain of  
627 the components as calculated in Debaille et al. (2006). The insert shows the location of the  
628 classical mantle end-members in the PC2 vs PC1 space.

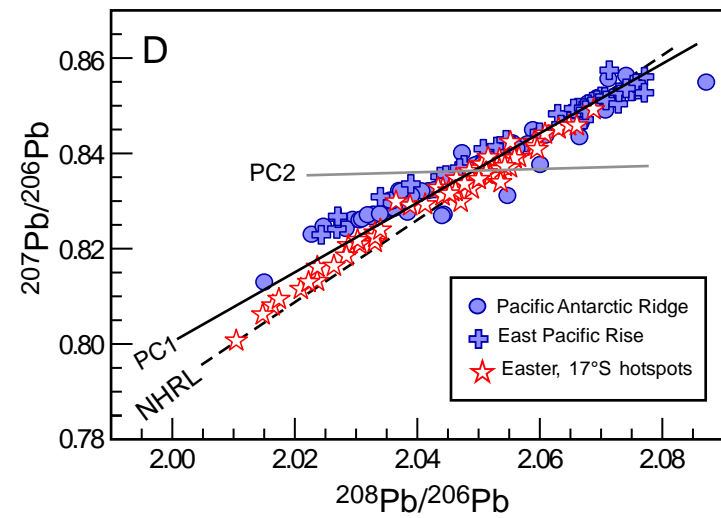
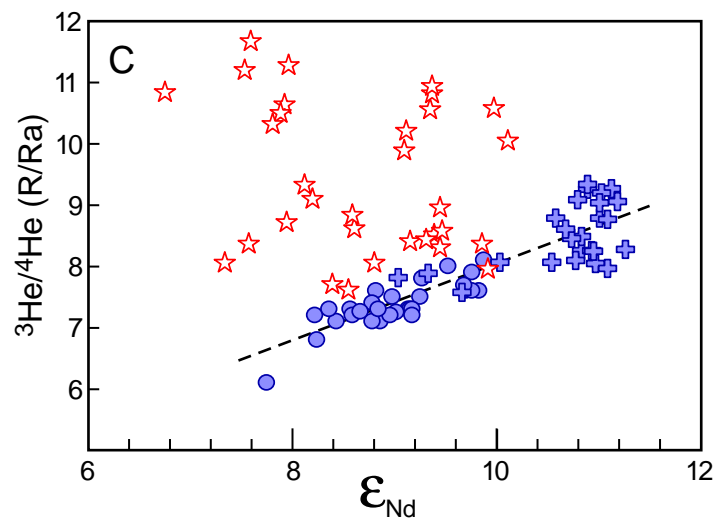
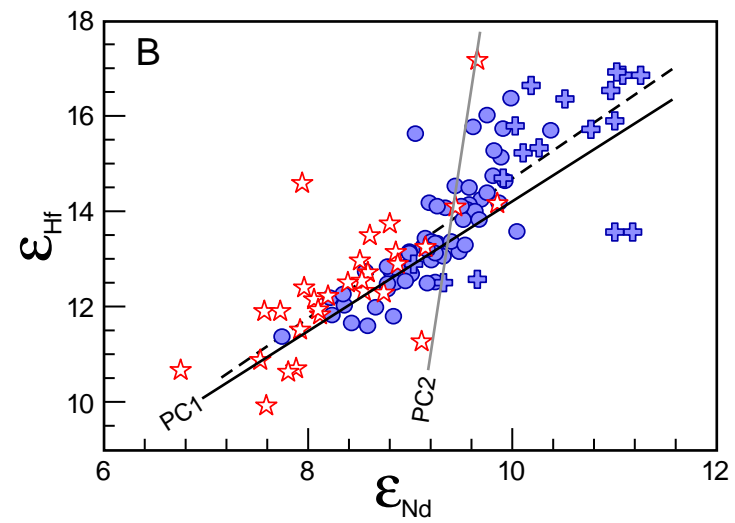
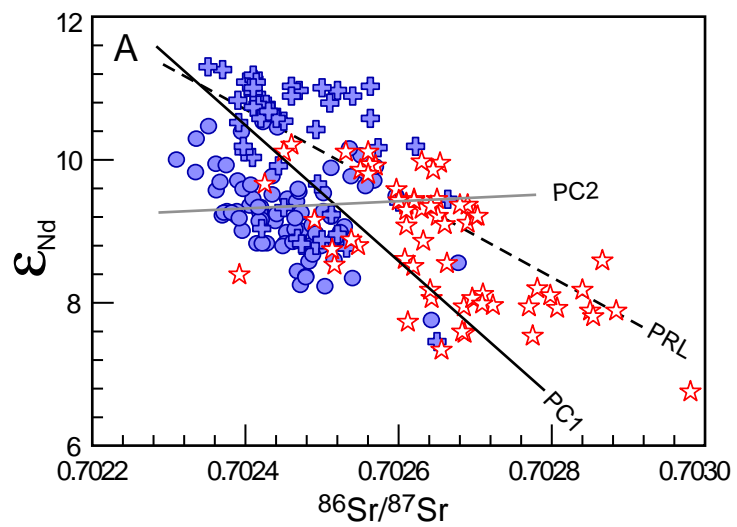
629

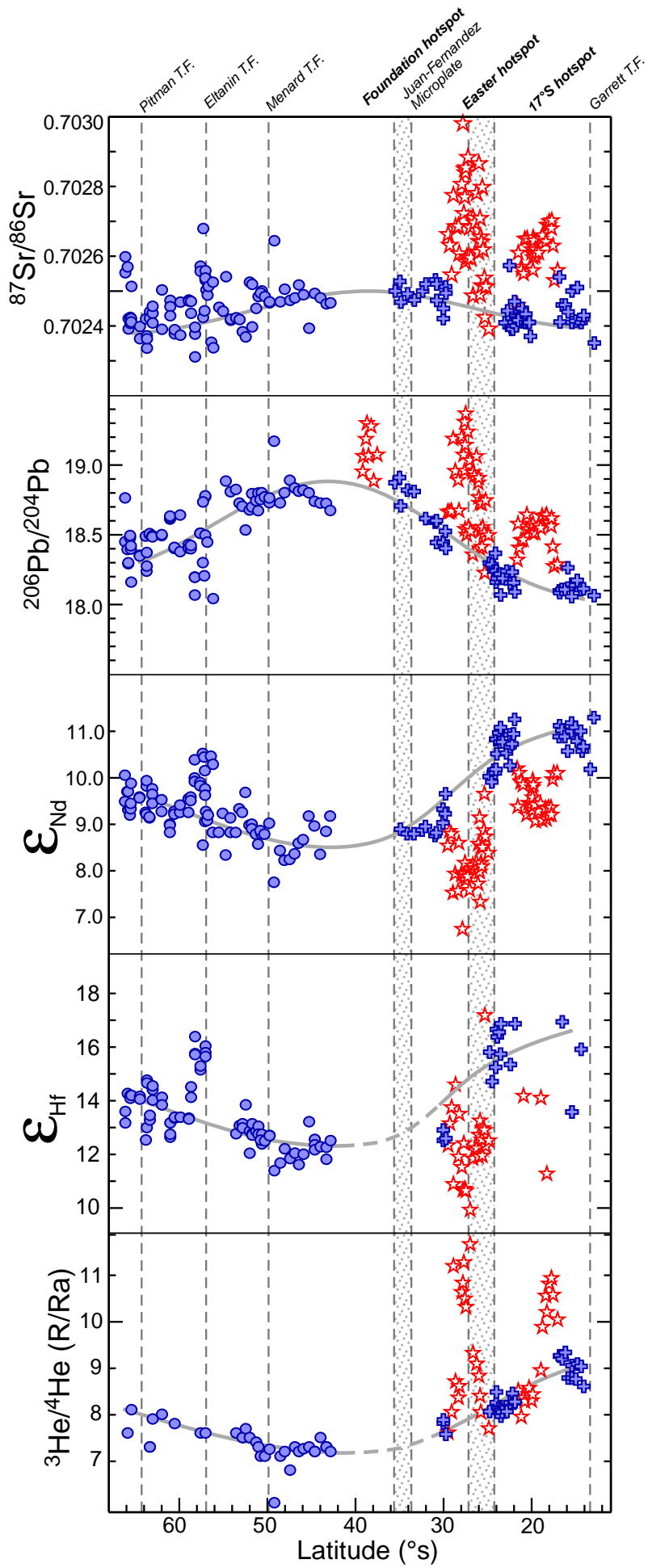
630 **Figure 6:** Binary plot of  $^3\text{He}/^4\text{He}$  vs  $^{206}\text{Pb}/^{204}\text{Pb}$ . The dashed regression line ( $^3\text{He}/^4\text{He} = -2.33$   
631  $^{206}\text{Pb}/^{204}\text{Pb} + 51.0$ ) is defined by samples devoid of plume influence. Plume-ridge interactions  
632 ( $17^\circ\text{S}$  and Easter hotspots) are characterized by positive trends emerging from the PAR-EPR  
633 array and pointing towards higher  $^3\text{He}/^4\text{He}$  (R/Ra) ratios and higher  $^{206}\text{Pb}/^{204}\text{Pb}$ .

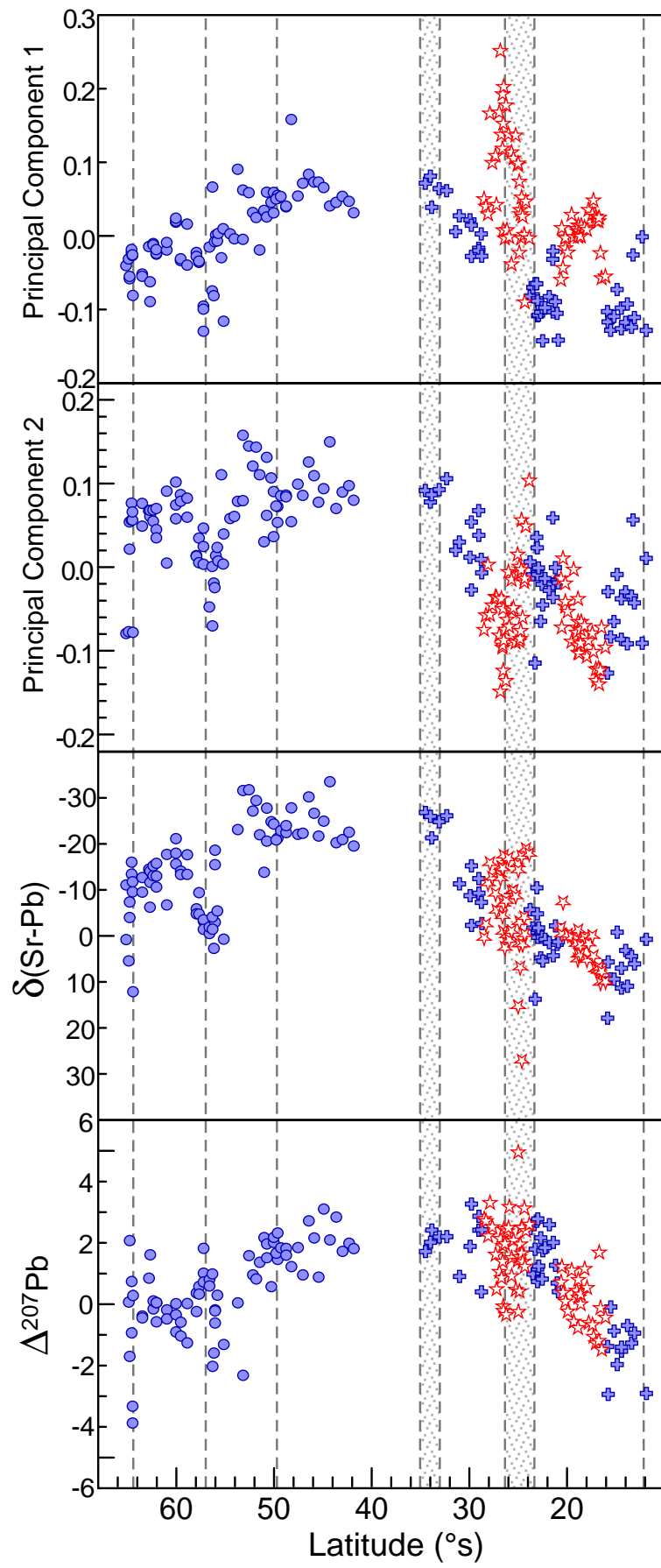
634

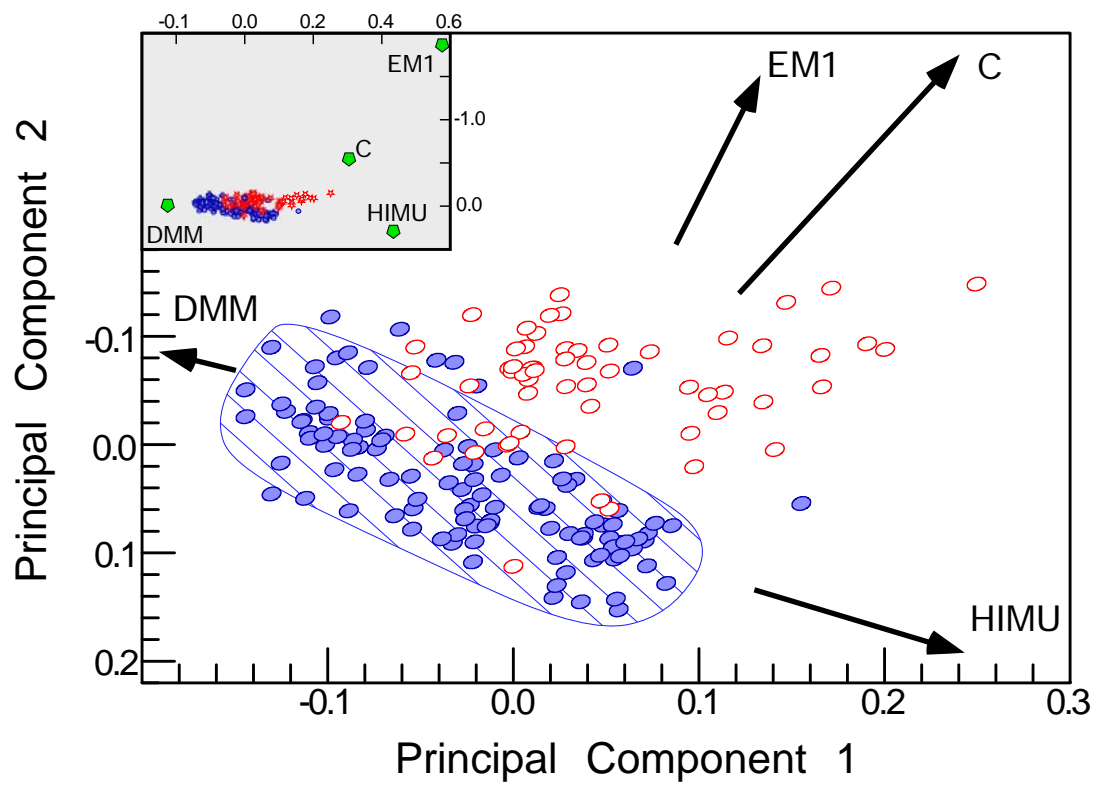
635 **Table 1:** Complete Sr, Nd, Pb, Hf and He isotope data table for PACANTARCTIC 1 and 2  
636 samples. In italic font, previously published data (Vlastélic et al., 1999; Vlastélic et al., 2000;  
637 Moreira et al., 2008; Hamelin et al., 2010).











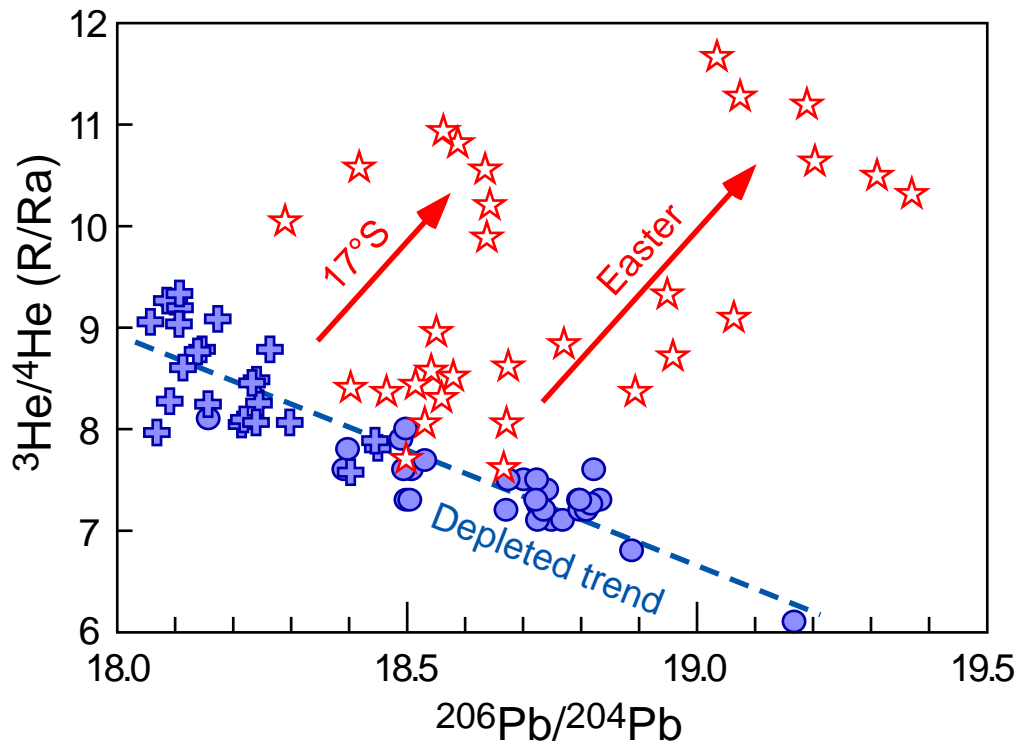


**Table 1:** Complete Sr, Nd, Pb, Hf and He isotope data table for PACANTARCTIC 1 and 2 samples. In italic font, previously published data (Vlastélic et al., 1999; Vlastélic et al., 2000; Moreira et al., 2008; Hamelin et al., 2010).

	$^{87}\text{Sr}/^{86}\text{Sr}$	$^{143}\text{Nd}/^{144}\text{Nd}$	$\epsilon_{\text{Nd}}$	$^{206}\text{Pb}/^{204}\text{Pb}$	$^{207}\text{Pb}/^{204}\text{Pb}$	$^{208}\text{Pb}/^{204}\text{Pb}$	$^{176}\text{Hf}/^{177}\text{Hf}$	$\epsilon_{\text{Hf}}$	$^3\text{He}/^4\text{He}$	Long. (°)	Lat. (°)	Depth
<b>PACANTARCTIC 2</b>												
PAC2DR38-1	<i>0.702465</i>	<i>0.513108</i>	9.17	18.671	15.533	38.039	<i>0.283125</i>	<i>12.50</i>	7.2	-111.3	-41.80	2524
PAC2DR37-1	<i>0.702462</i>	<i>0.513091</i>	8.84	18.722	15.540	38.110	<i>0.283106</i>	<i>11.80</i>	7.3	-111.3	-42.27	2475
PAC2DR37-2							<i>0.283118</i>	<i>12.25</i>	7.3	-111.3	-42.27	2475
PAC2DR36-1	<i>0.702479</i>	<i>0.513066</i>	8.34	18.724	15.538	38.117	<i>0.283119</i>	<i>12.27</i>	7.5	-111.6	-42.95	2503
PAC2DR35-1a							<i>0.283121</i>	<i>12.34</i>	7.2	-111.8	-43.59	2463
PAC2DR35-2	<i>0.702492</i>	<i>0.513097</i>	8.95	18.736	15.550	38.146	<i>0.283127</i>	<i>12.54</i>	7.2	-111.8	-43.59	2463
PAC2DR34-1	<i>0.702392</i>	<i>0.513108</i>	9.17	18.798	15.549	38.234	<i>0.283145</i>	<i>13.20</i>	7.3	-112.0	-44.24	2467
PAC2DR33-1	<i>0.702488</i>	<i>0.513082</i>	8.66	18.817	15.562	38.236	<i>0.283111</i>	<i>11.99</i>	7.26	-112.3	-44.87	2374
PAC2DR32-1	<i>0.702516</i>	<i>0.513078</i>	8.58	18.809	15.539	38.202	<i>0.283100</i>	<i>11.60</i>	7.2	-112.4	-45.39	2384
PAC2DR31-3	<i>0.702479</i>	<i>0.513066</i>	8.36	18.833	15.554	38.242	<i>0.283112</i>	<i>12.03</i>	7.3	-112.7	-45.85	2414
PAC2DR30-1	<i>0.702472</i>	<i>0.513060</i>	8.24	18.887	15.565	38.311	<i>0.283106</i>	<i>11.83</i>	6.8	-112.9	-46.40	2345
PAC2DR29-1	<i>0.702504</i>	<i>0.513059</i>	8.22	18.798	15.538	38.208	<i>0.283117</i>	<i>12.19</i>	7.2	-113.1	-47.01	2407
PAC2DR28-2	<i>0.702468</i>	<i>0.513070</i>	8.43	18.725	15.539	38.121	<i>0.283102</i>	<i>11.66</i>	7.1	-113.3	-47.51	2489
PAC2DR27-1	<i>0.702643</i>	<i>0.513035</i>	7.74	19.168	15.581	38.624	<i>0.283094</i>	<i>11.37</i>	6.1	-113.4	-48.18	2359
PAC2DR22-1	<i>0.702465</i>	<i>0.513100</i>	9.01	18.726	15.539	38.153	<i>0.283131</i>	<i>12.69</i>	7.25	-113.6	-48.73	2413
PAC2DR22-3	<i>0.702468</i>			18.761	15.540	38.202	<i>0.283130</i>	<i>12.68</i>		-113.6	-48.73	2413
PAC2DR21-2	<i>0.702483</i>	<i>0.513088</i>	8.78	18.768	15.544	38.189	<i>0.283125</i>	<i>12.48</i>	7.1	-113.8	-49.26	2339
PAC2DR9-1	<i>0.702499</i>	<i>0.513088</i>	8.78	18.768	15.540	38.202	<i>0.283122</i>	<i>12.37</i>		-117.0	-49.59	2380
PAC2DR9-2				18.798	15.552	38.244	<i>0.283132</i>	<i>12.73</i>		-117.0	-49.59	2380
PAC2DR20-1	<i>0.702493</i>	<i>0.513092</i>	8.86	18.749	15.540	38.168	<i>0.283126</i>	<i>12.51</i>	7.1	-116.8	-49.73	2441
PAC2DR8-1	<i>0.702483</i>	<i>0.513077</i>	8.56	18.796	15.550	38.237	<i>0.283132</i>	<i>12.74</i>	7.3	-117.1	-49.99	2221
PAC2DR8-2				18.670	15.535	38.031	<i>0.283140</i>	<i>13.03</i>		-117.1	-49.99	2221
PAC2DR7-4	<i>0.702449</i>	<i>0.513088</i>	8.78	18.741	15.528	38.148	<i>0.283135</i>	<i>12.84</i>	7.4	-117.2	-50.25	2229
PAC2DR6-1	<i>0.702518</i>	<i>0.513094</i>	8.90	18.792	15.543	38.201	<i>0.283133</i>	<i>12.75</i>		-117.2	-50.70	2610
PAC2DR6-6	<i>0.702396</i>	<i>0.513099</i>	8.99	18.696	15.537	38.123	<i>0.283143</i>	<i>13.12</i>		-117.2	-50.70	2610
PAC2DR5-2g	<i>0.702524</i>	<i>0.513098</i>	8.97	18.674	15.537	38.110	<i>0.283135</i>	<i>12.85</i>	7.5	-117.4	-50.98	2784
PAC2DR4-2	<i>0.702367</i>	<i>0.513134</i>	9.68	18.531	15.513	37.942	<i>0.283163</i>	<i>13.83</i>	7.7	-117.8	-51.43	2409
PAC2DR3-1							<i>0.283139</i>	<i>12.97</i>	7.5	-118.0	-51.79	2397
PAC2DR3-3	<i>0.702382</i>	<i>0.513112</i>	9.25	18.701	15.526	38.092	<i>0.283143</i>	<i>13.12</i>	7.5	-118.0	-51.79	2397
PAC2DR2	<i>0.702417</i>	<i>0.513116</i>	9.32	18.724	15.530	38.110	<i>0.283141</i>	<i>13.06</i>		-118.1	-52.13	2405
PAC2DR1-1	<i>0.702422</i>	<i>0.513090</i>	8.81	18.822	15.547	38.199	<i>0.283133</i>	<i>12.75</i>	7.6	-118.4	-52.53	2323
<b>PACANTARCTIC 1</b>												
PAC1DR14-2	<i>0.702538</i>	<i>0.513138</i>	9.75	18.494	15.489	38.100	<i>0.283225</i>	<i>16.02</i>	7.6	-145.09	-56.00	2617
PAC1DR14-3	<i>0.702530</i>	<i>0.513102</i>	9.05	18.776	15.524	38.379	<i>0.283214</i>	<i>15.63</i>		-145.09	-56.00	2617
PAC1DR14-4	<i>0.702557</i>	<i>0.513131</i>	9.62	18.769	15.523	38.370	<i>0.283218</i>	<i>15.77</i>		-145.09	-56.00	2617
PAC1DR13-2g	<i>0.702556</i>	<i>0.513142</i>	9.82	18.508	15.503	37.954	<i>0.283204</i>	<i>15.28</i>	7.6	-145.74	-56.57	2674
PAC1DR13-3	<i>0.702570</i>	<i>0.513145</i>	9.89	18.508	15.505	37.963	<i>0.283200</i>	<i>15.14</i>		-145.74	-56.57	2674
PAC1DR12-1g	<i>0.702310</i>	<i>0.513150</i>	9.99	18.064	15.467	37.468	<i>0.283235</i>	<i>16.37</i>		-146.29	-57.18	2539
PAC1DR12-3g	<i>0.702375</i>	<i>0.513146</i>	9.91	18.194	15.473	37.627	<i>0.283217</i>	<i>15.74</i>		-146.29	-57.18	2539
PAC1DR12-3r	<i>0.702395</i>	<i>0.513170</i>	10.38	18.192	15.470	37.620	<i>0.283216</i>	<i>15.70</i>		-146.29	-57.18	2539
PAC1DR11-1g	<i>0.702435</i>	<i>0.513125</i>	9.50	18.420	15.491	37.877	<i>0.283171</i>	<i>14.11</i>		-146.80	-57.63	2500
PAC1DR11-3	<i>0.702469</i>	<i>0.513129</i>	9.58	18.397	15.491	37.816	<i>0.283182</i>	<i>14.50</i>		-146.80	-57.63	2500
PAC1DR10-1g	<i>0.702473</i>	<i>0.513112</i>	9.25	18.426	15.492	37.881	<i>0.283149</i>	<i>13.33</i>		-148.50	-57.89	2319
PAC1DR10-3	<i>0.702470</i>	<i>0.513127</i>	9.54	18.400	15.483	37.798	<i>0.283148</i>	<i>13.30</i>		-148.50	-57.89	2319
PAC1DR09-g	<i>0.702467</i>	<i>0.513120</i>	9.40	18.638	15.511	38.075	<i>0.283150</i>	<i>13.37</i>		-149.14	-58.85	2484
PAC1DR09-1	<i>0.702372</i>	<i>0.513112</i>	9.25	18.376	15.470	37.819				-149.14	-58.85	2484
PAC1DR08-2	<i>0.702388</i>	<i>0.513110</i>	9.21	18.406	15.480	37.827	<i>0.283150</i>	<i>13.37</i>		-150.02	-59.5	2365
PAC1DR08-3	<i>0.702376</i>	<i>0.513113</i>	9.27	18.398	15.475	37.809	<i>0.283149</i>	<i>13.33</i>	7.8	-150.02	-59.5	2365
PAC1DR07-1g	<i>0.702472</i>	<i>0.513099</i>	8.99	18.609	15.505	38.039	<i>0.283144</i>	<i>13.16</i>		-152.08	-60.00	2362
PAC1DR07-2g	<i>0.702454</i>	<i>0.513098</i>	8.97	18.620	15.509	38.062	<i>0.283129</i>	<i>12.63</i>		-152.08	-60.00	2362
PAC1DR07-3	<i>0.702428</i>	<i>0.513090</i>	8.82	18.631	15.501	38.041	<i>0.283132</i>	<i>12.73</i>		-152.08	-60.00	2362
PAC1DR06-g	<i>0.702502</i>	<i>0.513126</i>	9.52	18.498	15.491	37.911	<i>0.283163</i>	<i>13.83</i>	8	-153.21	-60.94	2527
PAC1DR06-2	<i>0.702389</i>	<i>0.513113</i>	9.27	18.491	15.493	37.912	<i>0.283171</i>	<i>14.11</i>		-153.21	-60.94	2527
PAC1DR05-1g	<i>0.702407</i>	<i>0.513132</i>	9.64	18.489	15.495	37.926	<i>0.283168</i>	<i>14.00</i>		-154.54	-62.00	2344
PAC1DR05-3	<i>0.702435</i>	<i>0.513138</i>	9.75	18.490	15.496	37.936	<i>0.283179</i>	<i>14.39</i>	7.9	-154.54	-62.00	2344
PAC1DR05-r	<i>0.702455</i>	<i>0.513122</i>	9.44	18.482	15.488	37.904	<i>0.283183</i>	<i>14.53</i>		-154.54	-62.00	2344
PAC1DR03-1	<i>0.702421</i>	<i>0.513107</i>	9.15	18.505	15.498	37.974	<i>0.283152</i>	<i>13.44</i>	7.3	-156.08	-62.32	2219
PAC1DR03-2	<i>0.702439</i>	<i>0.513106</i>	9.13	18.498	15.494	37.965	<i>0.283147</i>	<i>13.26</i>	7.3	-156.08	-62.32	2219
PAC1DR02-g	<i>0.702335</i>	<i>0.513141</i>	9.81	18.272	15.511	37.837	<i>0.283189</i>	<i>14.75</i>		-156.54	-62.64	2489
PAC1DR02-1	<i>0.702362</i>	<i>0.513147</i>	9.93	18.369	15.498	37.860	<i>0.283186</i>	<i>14.64</i>		-156.54	-62.64	2489
PAC1CV09	<i>0.702370</i>	<i>0.513110</i>	9.21	18.236	15.588	38.063	<i>0.283139</i>	<i>12.98</i>		-159.61	-62.66	2714
PAC1CV08	<i>0.702419</i>	<i>0.513112</i>	9.25	18.487	15.503	37.965	<i>0.283126</i>	<i>12.52</i>		-162.44	-62.77	2534
PAC1CV06-r	<i>0.702362</i>	<i>0.513128</i>	9.56	18.344	15.475	37.787	<i>0.283169</i>	<i>14.04</i>		-166.06	-63.45	2755
PAC1CV06-g	<i>0.702397</i>	<i>0.513129</i>	9.58	18.350	15.476	37.804	<i>0.283172</i>	<i>14.15</i>		-166.06	-63.45	2755
PAC1CV04-g	<i>0.702512</i>	<i>0.513144</i>	9.87	18.157	15.462	37.575	<i>0.283173</i>	<i>14.18</i>	8.1	-169.40	-64.4	2340
PAC1CV03-r	<i>0.702423</i>	<i>0.513109</i>	9.19	18.475	15.501	37.952	<i>0.283173</i>	<i>14.18</i>		-171.88	-64.53	2576
PAC1CV03-g	<i>0.702406</i>	<i>0.513117</i>	9.34	18.492	15.486	37.923	<i>0.283170</i>	<i>14.07</i>		-171.88	-64.53	2576
PAC1CV02-g	<i>0.702568</i>	<i>0.513135</i>	9.69	18.391	15.485	37.868	<i>0.283175</i>	<i>14.25</i>	7.6	-172.43	-64.83	2936
PAC1CV01-r	<i>0.702551</i>	<i>0.513153</i>	10.05	18.447	15.557	38.121	<i>0.283156</i>	<i>13.58</i>		-173.75	-65.10	2863
PAC1CV01-g	<i>0.702597</i>	<i>0.513124</i>	9.48	18.761	15.591	38.549	<i>0.283144</i>	<i>13.16</i>		-173.75	-65.10	2863

## Supplementary Material

### *New algorithm to compute a PCA:*

The PCA method is a linear transformation that converts the data into a new coordinate system in which the direction along which the greatest data variance is expressed, becomes the first axis (PC1). The direction along which the greatest data variance is expressed orthogonal to PC1 becomes the second axis (PC2), and so on. The first step, called the whitening, consists in normalizing the data. This is done by subtracting the mean value from each data point and dividing the result by the standard deviation of each variable. The correlation matrix (Pearson's correlation matrix) of the reduced variables can then be calculated. The next step consists into diagonalizing the correlation matrix in order to find the eigenvalues, which correspond to the dimensions that have the strongest correlation in the data set. The principal components are the coordinates of the data points in the eigenvector referential.

The PCA method used with our geochemical dataset has been initially developed for low-rank matrix approximations (Srebro and Jaakkola, 2003) and was recently adapted for tectonic problems using incomplete geodetic times series (Kositsky and Avouac, 2010). The algorithm used to compute our principal components has been written specifically to address the major problem of a geochemical database: missing data in the matrix. Traditionally, for a given sample, it is necessary to acquire as many different isotope measurements as the number of dimensions used in the PCA. The paucity of combined Sr-Nd-Pb-Hf isotope data in individual samples is therefore an important issue for standard PCA algorithms. The more dimensions we use in the PCA, the fewer samples meet the required conditions: from 210 samples for 2-dimension (Sr-Nd) space to only 99 samples for a 6-dimension space. The main difference with a classical PCA is that we have replaced the standard Singular Value Decomposition (SVD) with a more sophisticated decomposition proposed by Srebro and Jaakkola [2003]. In this approach the data matrix  $X$  is decomposed into components  $U$ ,  $S$ ,  $V$ , with each data point weighted according to the square of its standard error. This decomposition is particularly adapted to take into account individual measurement errors and deal with missing data points. It allows us to compute the Principal Components on the entire data set, even if some isotopic ratios are missing. Each missing data point is weighted with infinite standard error. We want to emphasize that, consequently, no interpolation is made, which could erase some local effect. This technique is particularly suitable to geochemical data as it allows us to complete the principal components using the whole dataset, increasing therefore the accuracy of the calculation.

## *Limits of PCA:*

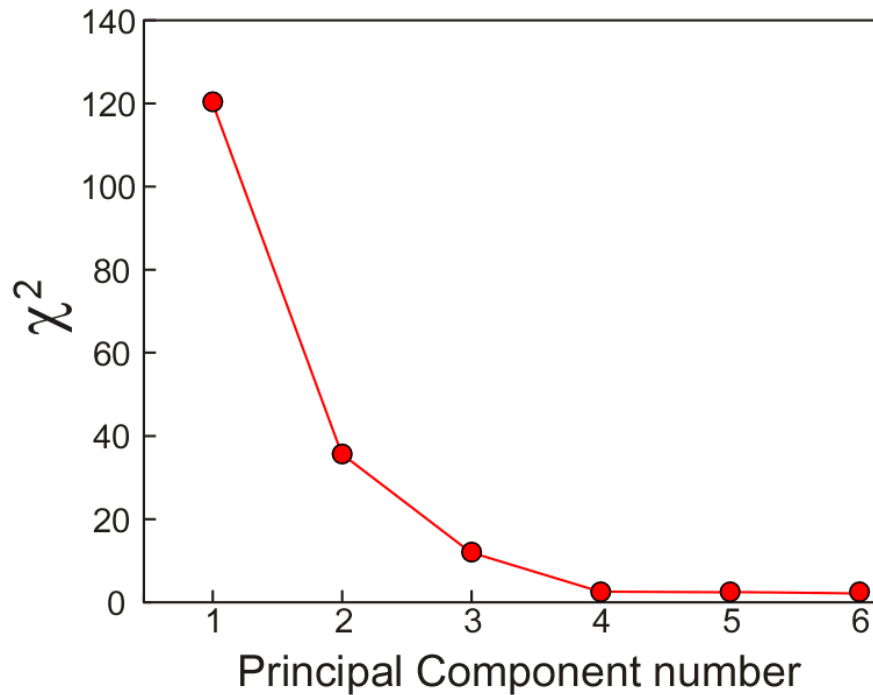
### *Classical limits related to PCA calculation:*

Because the PCA method is an orthogonal linear transformation, it assumes the linearity of the data co-variations. In most binary isotopic diagrams, mixing processes are expressed by hyperboles whose curvatures depend on the elemental concentration ratios of the involved end-members. But in the case of MORB, pseudo-linear correlations are observed (Fig. 2) indicating that denominator elements are in approximately constant proportions in the mixing components. It is very difficult to evaluate the extent of non-linear relationships concealed within the analytical noise. However, it is interesting to note that the geographical variations of the components calculated with our method are approximately the same as those computed in the 3-dimensional space of Pb isotopes, in which relationships are linear. In order to minimize the correlations induced by the  $^{204}\text{Pb}$  analytical noise (it represents only about 1.4% of the total Pb), the computation has been made in the  $^{204}\text{Pb}/^{206}\text{Pb}$ ,  $^{207}\text{Pb}/^{206}\text{Pb}$  and  $^{208}\text{Pb}/^{206}\text{Pb}$  space. Considering the problematic of our study, this observation suggests that the curvature can be neglected.

### *Limits related to our new algorithm:*

Compared to traditional PCA algorithms, principal components are computed here altogether rather than separately, because the number of components affects the subspace in which these components reside. A limit to this method appears if one variable is represented by fewer samples than compared to other variables. In this particular case, a sample with a value corresponding to this “rare” variable is artificially given more weight. In return, each variable is also weighed in proportion to its number of samples. Because the number of He isotope analyses along the studied ridge section is too low compared to other isotopes, the information provided by this parameter has not been included in the PCA calculation.

*Distribution of the variance among the principal components:*



Plot of the residual variance ( $\chi^2$ ) versus the principal component number

*Figure 2 data references:*

Bach, W., Hegner, E., Erzinger, J., Satir, M., 1994. Chemical and isotopic variations along the superfast spreading East Pacific Rise from 6° S to 30° S. *Contribution to Mineralogy and Petrology*, 116(4): 365-380.

Castillo, P., 1988. The Dupal anomaly as a trace of the upwelling lower mantle. *Nature*, 336: 667-670.

Fontignie, D., Schilling, J.-G., 1991. <sup>87</sup>Sr/<sup>86</sup>Sr and REE variations along the Easter Microplate boundaries (south Pacific): Application of multivariate statistical analyses to ridge segmentation. *Chemical Geology*, 89: 209-241.

Hanan, B.B., 1989. Easter Microplate evolution: Pb isotope evidence, *Journal Geophysical Research*, 94: 7432-7448.

Kingsley, R.H., Blichert-Toft, J., Fontignie, D., Schilling, J.G., 2007. Hafnium, neodymium, and strontium isotope and parent-daughter element systematics in basalts from the plume-ridge

- interaction system of the Salas y Gomez Seamount Chain and Easter Microplate. *Geochem Geophys Geosyst*, 8: 28.
- Kurz, M.D., Moreira, M., Curtice, J., Lott III, D.E., Mahoney, J.J., Sinton, J.M., 2005. Correlated helium, neon, and melt production on the super-fast spreading East Pacific Rise near 17°S. *Earth Planet. Sci. Lett.*, 232(1-2): 125-142.
- Mahoney, J.J., Sinton, J.M., Kurz, M.D., Macdougall, J.D., Spencer, K.J., Lugmair, G.W., 1994. Isotope and trace element characteristics of a super-fast spreading ridge: East Pacific Rise 13-23°S. *Earth Planet. Sci. Lett.*, 121: 173-193.
- Maia, M., C. Hemond and P. Gente 2001. Contrasted interactions between plume, upper mantle, and lithosphere: Foundation chain case. *Geochem Geophys Geosyst* 2: U25-U53.
- Niu, Y.L., Waggoner, D.G., Sinton, J.M., Mahoney, J.J., 1996. Mantle source heterogeneity and melting processes beneath seafloor spreading centers: The East Pacific Rise, 18 degrees-19S. *Journal of Geophysical Research*, 101(B12): 27711-27733.
- Nowell, G.M., Kempton, P.D., Noble, S.R., Fitton, J.G., Saunders, A.D., Mahoney, J.J., Taylor, R.N., 1998. High precision Hf isotope measurements of MORB and OIB by thermal ionisation mass spectrometry: insights into the depleted mantle. *Chemical Geology*, 149(3-4): 211-233.
- Vlastélic, I., Dosso, L., Guillou, H., Bougault, H., Geli, L., Etoubleau, J., Joron, J.L., 1998. Geochemistry of the Hollister Ridge: relation with the Louisville hotspot and the Pacific-Antarctic Ridge. *Earth Planet. Sci. Lett.*, 160(3-4): 777-793.
- White, W.M., Hofmann, A.W., Puchelt, H., 1987. Isotope geochemistry of Pacific mid-ocean ridge, *Journal Geophysical Research*, 92: 4881-4893.